Penetration Phenomena at Relativistic Energies

U.I. Uggerhøj*

Department of Physics and Astronomy, University of Aarhus
DK-8000 Aarhus C, Denmark

Abstract

A number of different penetration phenomena for relativistic particles are presented. Included in the discussion are subjects like the Chudakov effect, nuclear size effect, heavy ion pair production and bremsstrahlung, fragmentation, nuclear-charge pickup, penetration in bent and straight crystals and formation zone effects such as the Landau–Pomeranchuk–Migdal effect and the Ternovskii–Shul'ga–Fomin effect.

Contents

* E-mail: ulrik@phys.au.dk

1. Introduction

A thorough understanding of penetration phenomena is essential to a wide range of applications, ranging from detector construction to semiconductor fabrication. In the present review, the attention is restricted to penetration phenomena for relativistic particles, i.e. particles for which the kinetic energy E exceeds the rest mass m. In this case, the Lorentz factor $\gamma = E/mc^2$ becomes significantly larger than unity, and stopping phenomena not observed at lower energies become relatively important. Two examples are nuclear charge pick-up mediated by a $\gamma n \to p\pi^-$ reaction through virtual photons and radiative energy loss or its "symmetric" counterpart, pair production.

The emphasis in this review will be on presenting in a short form the relevant modifications to standard formulae, with references given to sources where such effects were first derived or observed as well as to sources with more rigour, rather than full derivations of the formulae or detailed surveys of the experiments. In this connection, it is attempted to discuss the physics contents of the presented effects and an estimate of their relavance to other areas. The presentation is by no means exhaustive, but reflects the personal interests of the author.

2. Ionization Energy Loss

It is shown in a number of treatments (Sigmund, 2006; Yao et al., 2006; Jackson, 1975) that the energy loss owing to the ionization during penetration of a medium at high energies is given by the Bethe formula

$$-\frac{\mathrm{d}E}{\mathrm{d}x} = \frac{4\pi N Z_1^2 Z_2 e^4}{m\beta^2 c^2}\left(\frac{1}{2}\ln\frac{2mc^2\beta^2\gamma^2 T_{\max}}{I^2} - \beta^2 - \frac{\delta(\beta\gamma)}{2}\right), \tag{1}$$

where $Z_1 e$ is the charge of the projectile, $Z_2 e$ is the charge of the lattice nuclei, N the atomic density, I the ionization potential and $T_{\max} = 2mc^2\beta^2\gamma^2/(1 + 2\gamma m/M + (m/M)^2)$ is the maximum kinetic energy which can be transferred to a free electron of rest mass m in a single collision with a projectile of mass M and Lorentz factor $\gamma = 1/\sqrt{1-\beta^2}$ (Yao et al., 2006). The last term in Equation (1) is the density effect correction, to be discussed below.

2.1. Restricted Energy Loss

In a number of different experiments, it is not the energy loss of the penetrating particle that is of main interest, it is rather the energy *deposited* in the substance that is measured. Part of the energy loss suffered by the projectile may e.g. appear in the form of energetic knock-on electrons (electrons escaping the medium with high energy as a result of a binary collision with the projectile). This happens for instance when this – so-called restricted – energy loss is measured in a silicon surface-barrier detector. In this case, an equation similar to Equation (1) applies, but with $T_{\max}$ replaced by the smaller value T_{cut} (corresponding to the smallest energy sufficient for an electron to have a range of half the target thickness) and the second term in the square bracket, β^2, modified by a multiplier $(T_{\mathrm{cut}} + T_{\max})/2$. At relativistic energies, the restricted energy loss in e.g. silicon is $\simeq$ 330 keV/mm for not too thick targets.

2.2. Density Effect – Fermi Plateau

As is also discussed in a number of excellent textbooks (Sigmund, 2006; Yao et al., 2006; Jackson, 1975), the Lorentz contraction of the electric field as seen from the target frame makes distant collisions more important at increasing energies. However, at sufficiently large distances, the medium acts as a dielectric, changing the electromagnetic field of the penetrating particle from its value in vacuum thus reducing the contribution from the distant collisions. At very high energies the replacement

$$\frac{\delta(\beta\gamma)}{2} \to \ln\frac{\hbar\omega_p}{I} + \ln(\beta\gamma) - \frac{1}{2} \tag{2}$$

in Equation (1) must be made (Yao et al., 2006), where ω_p is the plasma frequency. This replacement corresponds to a much slower rise of the stopping power with increasing energy than in the case without density effect.

2.3. Chudakov Effect

A considerable contribution to the ionization energy loss originates from large transverse distances, $b_q \simeq v/\omega_p$. If a penetrating assembly of separate charges are internally spaced less than this distance, the ionization is influenced by interference terms from the charges. This can be the case e.g. for an energetic hydrogen molecule that is stripped upon entry to the substance, but it can also be an effect present for a electron-positron pair where each participating charge screens the charge of the other as seen from the relevant distance b_q in the medium. The energy loss thus diminishes close to the creation point if the created pair is sufficiently energetic and therefore forward directed. This is the so-called Chudakov effect. Under the assumption that the created pair moves in a straight line after creation, the only angle that contributes to the separation is the emission angle $1/\gamma_p$. Thus, after having traversed a distance given by

$$l_s = \frac{\beta\hbar\omega}{mc\omega_p}, \tag{3}$$

the pair from a photon of energy $\hbar\omega$ would be separated by $b_q = v/\omega_p$.

This would result in a reduced restricted energy loss at distances smaller than about l_s from the creation vertex, due to internal screening. The result from the destructive interference term is a (restrictive) energy loss of the pair (Berestetskii and Geshkenbain, 1956; Akhiezer and Shul'ga, 1996)

$$\frac{\mathrm{d}E_\pm}{\mathrm{d}t} = 2\frac{\alpha\hbar\omega_p^2}{\beta}\left[\ln\frac{\sqrt{2mc^2T_{(\mathrm{cut})\,\max}}}{\hbar\omega_p} - K_0\left(\frac{s\omega_p}{\beta c}\right)\right], \tag{4}$$

where $K_0(x)$ is the modified Bessel function of the second kind with order zero and s is the transverse separation of the pair which exceeds the longitudinal separation by a factor γ. As usual, the plasma frequency is given from $\omega_p^2 = 4\pi N Z_2 e^2/m$ where NZ_2 is the number density of electrons.

For small separations s the modified Bessel function can be approximated by $K_0(x) \simeq \ln(1/x)$ which results in

$$\frac{\mathrm{d}E_\pm}{\mathrm{d}t} \simeq 2\,\frac{\alpha\hbar\omega_p^2}{\beta}\ln\left(s\sqrt{2mc^2T_{\mathrm{cut}}}\right) \tag{5}$$

at small distances from the vertex. For large separations the modified Bessel function tends exponentially to zero, corresponding to loss of effective internal screening, and twice the standard expression for the stopping power at high speed in a Fermi gas, see e.g. Sigmund (2006, equation (5.165)), is retrieved from Equation (4).

In principle, in order to convert from internal separation s to traversed distance x, the emission angle $y_e = x/\gamma_p$ and multiple Coulomb scattering (Yao et al., 2006) contributions

$$y_m = \sqrt{\frac{2}{3}}x\theta_0 = \sqrt{\frac{2}{3}}x\,\frac{13.6\ \mathrm{MeV}}{\beta cp}\sqrt{\frac{x}{X_0}}\left(1 + 0.038\ln\frac{x}{X_0}\right) \tag{6}$$

must be added. However, since the multiple scattering is affected by the internal screening as well, this contribution is usually neglected.

Figure 1 shows a calculation of the relative reduction in (restricted) energy loss during the penetration of a gold foil. Clearly, according to Equation (3), foils with smaller plasma frequencies would be preferable, but since pair creation is roughly proportional to Z_2^2 it is advantageous to use high-Z materials, of which gold is a good choice because of its structural properties. There have been a few measurements of the Chudakov effect from cosmic ray tracks in emulsions (Perkins, 1955; Jain, 1962) – about a dozen in total – and at least one proposal for a measurement in an accelerator environment (Zielinski, 1985). However, most of such proposals seem to forget the inherent noise contribution from thin solid-state detectors, originating from the capacitance.

A closely related effect has recently been calculated for Cherenkov radiation emission from e^+e^- pairs in the vicinity of the creation point (Mandal et al., 2005). This internal screening effect may affect decisively the behaviour of the Cherenkov emission in neutrino-induced electromagnetic showers.

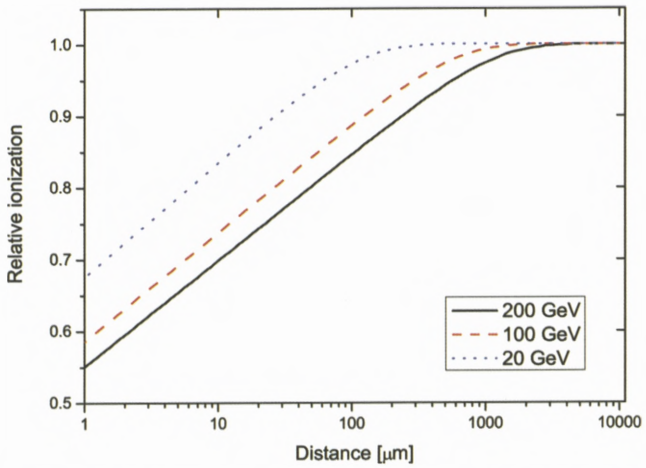

Figure 1. The relative reduction in (restricted) energy loss during the penetration of a gold foil as a function of penetration length for 200, 100 and 20 GeV electron-positron pairs.

2.4. Ionization Energy Loss for Ions

2.4.1. *Nuclear Size Effect*

Once the de Broglie wavelength of the electron impinging on the projectile nucleus – as seen from the frame of the penetrating particle – becomes of the order of the nuclear size or smaller, the stopping force diminishes. Alternatively, expressed as in the original paper by Lindhard and Sørensen (1996), once the angular momentum corresponding to an encounter with the nucleus γmcR exceeds $\hbar/2$ where $R = 1.2 \text{ fm} \cdot A^{1/3}$ is the nuclear radius, A being the projectile mass number, the phase shift compared to the point nucleus case becomes modified. These conditions translate into a Lorentz factor

$$\gamma = \frac{\lambda\!\!\!^{-}}{2R} \simeq \frac{160}{A^{1/3}}, \tag{7}$$

beyond which the nuclear size becomes important for the stopping. Thus for $\gamma \gtrsim 27$, one can expect the nuclear size for lead to be significant, and an accurate evaluation shows that in the case of uranium, the influence of the finite nuclear size on the stopping becomes 1% already at $\gamma = 10$ (Lindhard and Sørensen, 1996). Even stronger effects from the finite nuclear size is expected in straggling, since it originates from close collisions. However, straggling measurements performed on relativistic ion beams have so far been completely dominated by multiple Coulomb scattering, such that firm conclusions were excluded (Datz et al., 1996).

2.4.2. *Free-Free Pair Production and Bremsstrahlung*
Apart from the nuclear size effect in stopping, there remains the possibilities of the penetrating ion producing bremsstrahlung and/or pair creation. Both of these processes may contribute to the slowing down of the projectile and have been treated theoretically by Sørensen (2003, 2005). In Sørensen (2003) it is shown that the discrepancy between measured values (Datz et al., 1996) and theoretical values including the nuclear size effect (Lindhard and Sørensen, 1996) is likely to be due to energy loss originating from pair production in the screened nuclear field. In Sørensen (2005) it is shown that the condition that the projectile stays intact during the slowing down process, is in fact a very restrictive one. It limits the bremsstrahlung emission which in this treatment amounts to a few permille of the stopping power related to pair production. Thus, for bare lead on a lead target, Sørensen found that the stopping force related to pair production becomes dominant compared to the ionization contribution for γ exceeding a few 10^3, with the bremsstrahlung channel constantly being much smaller.

2.4.3. *Bound-Free Pair Production*
A closely related effect appears in electron capture by relativistic heavy ions where one of the contributing channels is bound-free pair production instead of free-free as above. This effect is of particular interest to the heavy ion collider community since it may limit the lifetime of stored heavy ion beams – an ion capturing an electron no longer has the correct charge per momentum to stay within the machine acceptance.

There are three mechanisms for the ion to capture an electron: Radiative electron capture (REC), non-radiative electron capture (NRC) and electron capture from pair production (ECPP). In ECPP, the pair is created in the strong electromagnetic field of the interaction with the target nucleus, the electron is captured, while the positron is lost. The REC and NRC processes become of less importance than ECPP for projectiles with $\gamma \gtrsim 100$. Measurements have been performed of the cross section for ECPP summed over all final nl states (Krause et al., 2001). Surprisingly, these measurements agree very well with theoretical values for capture to the $1s$ state only, although capture to higher states are expected to yield a $\simeq 30\%$ increase. This discrepancy is not understood.

2.5. Ionization Energy Loss for Channeled Ions

For channeled particles (the channeling phenomenon is introduced in more detail below), a path-dependent average energy loss for relativistic particles was calculated by Esbensen and Golovchenko (1978)

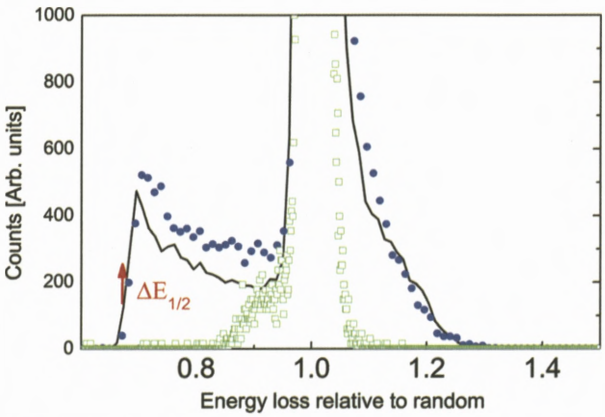

Figure 2. Energy-loss distribution for 33 TeV fully stripped lead nuclei penetrating a silicon single crystal along the (110) plane. The full-drawn curve represents the simulated values for energy loss in this orientation, the filled dots the results for the oriented crystal and the open squares the results for the randomly oriented crystal (Møller et al., 2001). The minimum energy loss for channeled particles $\Delta E_{1/2}$ is indicated by the arrow.

$$\frac{\mathrm{d}E}{\mathrm{d}x}(\mathbf{b}) = \frac{2\pi e^4 N}{mv^2} Z_1^2 \left[\big(Z_2 + Z_2(\mathbf{b})\big) \ln \frac{2mv^2\gamma^2}{I} + C(\mathbf{b}) \right], \tag{8}$$

where $NZ_2(\mathbf{b})$ is the local electron density at position $\mathbf{b}$ in the transverse plane and $C(\mathbf{b})$ is a velocity-independent term dependent on the local electron density at position b. The terms $(Z_2 + Z_2(b))\beta^2$ and $Z_2\delta$ were added in the square parenthesis to include relativistic effects (Esbensen et al., 1978). Also the reduction in the well-defined leading edge $\Delta E_{1/2}$ of the energy-loss distribution for channeled particles was calculated to be (Esbensen et al., 1978)

$$\left(\frac{\mathrm{d}E}{\mathrm{d}x}(\mathbf{b})\right)_{1/2} = \left(\frac{\mathrm{d}E}{\mathrm{d}x}(\mathbf{b})\right) + \frac{2\pi e^4 N}{mv^2} Z_1^2 Z_2(\mathbf{b}) \big[-1.18 + \beta^2 + \ln \kappa(\mathbf{b}) \big], \tag{9}$$

where

$$\kappa(\mathbf{b})) = \frac{2\pi e^4 N}{mv^2} Z_1^2 Z_2(\mathbf{b}) \frac{t}{T_{\max}}. \tag{10}$$

In Figure 2 the energy-loss distribution is shown for 33 TeV fully stripped lead nuclei penetrating a silicon single crystal along the (110) plane. The single crystal is acting as an active target, measuring the restricted energy loss for the channeled and above-barrier (random) particles. The full-drawn curve represents the simulated values for energy loss in this orientation, the filled dots the results

for the oriented crystal and the open squares the results for the randomly oriented crystal (Møller et al., 2001). From the results of the simulation, split into transverse energy components, it is shown that the right-hand edge corresponding to energy loss above that of the random orientation, originates from transverse energies close to the barrier height, 20–25 eV. Conversely, the left-hand edge, corresponding to energy losses approaching 60% of that of the random orientation, stems from ions channeled deep in the potential well, 0–5 eV transverse energy, as expected (Møller et al., 2001). The minimum energy loss for channeled particles $\Delta E_{1/2}$ is well described by the theory developed by Esbensen and coworkers (Esbensen et al., 1978; Esbensen and Golovchenko, 1978), as indicated by the arrow in Figure 2.

For the channeled ions, close encounter processes are heavily suppressed and the nuclear size effect as well as pair production are not expected to play a significant role.

3. Fragmentation

In order to facilitate an efficient design of a collimation system for the CERN Large Hadron Collider (LHC) operating as an ion-collider, it is necessary to test nuclear fragmentation models in a wide range of masses and energies of colliding nuclei. This must be done to make the foundation for an extrapolation to higher beam energies as solid as possible and thus reduce the likelihood of e.g. superconducting magnet quench as a result of interception of fragments. In comparison to the LHC operating with protons, collimation of heavy ions in the LHC is a complex task (Jowett et al., 2003). The reason for this is the traditional division into primary and secondary collimators where the primary in the case of protons almost exclusively acts as a scatterer and the secondary intercepts the scattered particles (Jeanneret, 1998). In the case of ions, the primary collimator to a large extent generates fragments, the motion and distribution of which are much less well known than multiple scattering distributions. Thus, systematic experimental tests of fragmentation models over a wide range of beam energies, targets and/or projectiles are needed to determine the accuracy of such models. Fragmentation and nuclear-charge pick-up reactions for ultrarelativistic Pb in a variety of targets have been investigated. Predictions of several fragmentation models (Scheidenberger et al., 2002, 2004) compared quite well to the experimental data.

The data and calculations for indium shown in Figure 3 show a nice agreement in shape as well as for the absolute value. The cross sections for nuclear-charge pickup channel forming $_{50}$Sn nuclei were also measured and calculated. This

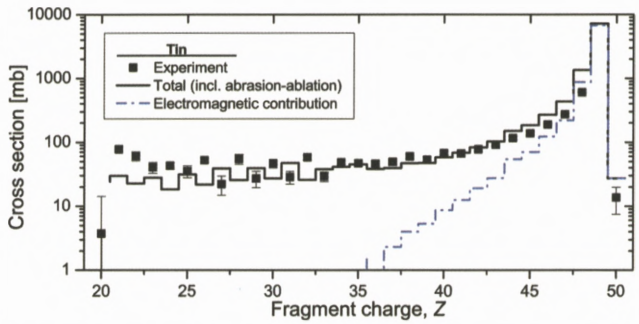

Figure 3. Fragmentation cross sections for ultrarelativistic In on Sn. The filled squares represent the measured values, the full line is the total expected cross section based on the abrasion-ablation model including the electromagnetic contribution and the dash-dotted line is the electromagnetic contribution alone (Uggerhøj et al., 2005b).

process is attributed to the electromagnetic production of a negative pion by an equivalent photon as will be discussed in the next section.

3.1. Nuclear-Charge Pickup

Many experiments have found evidence for electromagnetic processes in reaction channels, where either the fragment mass A and/or the fragment atomic number Z were lower than those of the incoming projectile. Those channels are by far the dominating ones due to the large number of conceivable (hadronic and electromagnetic) processes, which all lead to a reduction in Z and/or A (such as knockout, sequential breakup, evaporation, etc.). This has been discussed in the section on fragmentation. In rare cases, however, the nuclear charge Z of the projectile is increased, a process which in the following will be called nuclear charge pickup, $\Delta Z = +1$. Such reactions can be explained at low energies, below the Fermi energy in nuclei, by proton transfer through the nuclear overlap zone. At relativistic energies, however, the Fermi spheres of projectile and target are never overlapping, which prevents transfer of, e.g., a target proton to the projectile. Instead, one process that may lead to nuclear charge pickup is Δ-resonance formation and decay in nucleon-nucleon collisions. For intermediate energies, $\gamma \lesssim 10$, this is the most likely elementary process in which a projectile neutron can be converted into a proton, e.g., by $n \to \Delta^0 \to p + \pi^-$ with subsequent absorption of the proton in the projectile and emission of the π^-. At ultrarelativistic energies, $\gamma \gtrsim 100$, a different mechanism of nuclear-charge-changing interactions between heavy ions becomes significant. This channel opens, because the maximum equivalent photon energy, $E_{\max} = \gamma\hbar c/b_c$, exceeds the pion production

threshold of 140 MeV, b_c being the minimum impact parameter in electromagnetic interactions. In collisions using 158 GeV per nucleon Pb projectiles, the maximum equivalent photon energy exceeds the pion production threshold by factors of 20 to 40, depending on the target. A π^- produced in such a reaction, $\gamma n \rightarrow \pi^- p$, may be emitted while the associated proton may be captured to form a residual nucleus with $\Delta Z = +1$ compared to the projectile. In general, this resulting nucleus is highly excited and is likely to deexcite by neutron evaporation. Measurements with 158 GeV per nucleon Pb (Scheidenberger et al., 2002, 2004) and 158 GeV per nucleon In projectiles (Uggerhøj et al., 2005b) were performed, yielding results in good agreement with elaborate calculations for the nuclear charge pick-up, based on the Weizsäcker–Williams method of virtual quanta.

3.2. Some Remaining Puzzles and Problems

For the subject of ionization energy loss, an experimental proof of the Chudakov effect in an accelerator based beam is still lacking. With cosmic ray investigations, the total number of observed suppressed events is less than about a dozen. Another interesting question is if the straggling is affected by the nuclear size. However, as discussed above, the competing mechanism of beam broadening – multiple Coulomb scattering – has so far prohibited trustworthy conclusions to be drawn from data. On the other hand, there is nothing fundamental prohibiting such a measurement which may also shed light on the explanation of the remaining small discrepancy between energy loss data and theory including the nuclear size. Concerning the theory of the nuclear size effect, a more accurate potential than the square well potential for the nuclear term (like a Woods–Saxon potential) is not expected to lead to any significant alteration of the calculated values for the nuclear size effect. The important distance in this effect is the (reduced) Compton wavelength, and small changes on the scale of nuclear distances, about two orders of magnitude smaller, will be almost completely insignificant.

For the subject of fragmentation of heavy ions, the bremsstrahlung spectrum from a heavy ion has not yet been observed nor have positrons with energies above 10 MeV. Is the pair production the origin of the discrepancy between experimental values for the energy loss of heavy ions and theory including the nuclear size effect as Sørensens calculations indicate?

For ECPP the experiment includes capture to all states, whereas theoretical values are calculated for capture to the 1s state only. The convincing agreement between theory and experiment may therefore be fortuitous.

4. Bent Crystals

The guidance of channeled particles in a crystal persists even if the crystal is slightly bent, such that the particle may be deviated from its original direction of motion as in a magnetic dipole. Since the fields that are responsible for this deviation are the extremely strong fields present near the lattice nuclei, the corresponding bending strength can reach a magnitude of the equivalent of several thousand Tesla. It is therefore possible to design a crystalline "kicker" with an equivalent deflection power of 10 Tm by use of a device that is of the order 0.1 m long.

In Baurichter et al. (2000) a concise introduction to the field is given along with a summary of the results obtained at the CERN SPS. In these texts extensive reference lists are included. For a short introduction to the field, see Møller (1995).

4.1. Critical Curvature

There is a certain curvature at which the particles will dechannel in a bent crystal due to the centrifugal force that tends to increase the interactions with the lattice nuclei. Estimating this curvature, it was found in the late seventies that as long as the curvature fulfills the condition:

$$\kappa \leq \kappa_c = \frac{\pi Z_1 Z_2 e^2 N d_p}{pv} \tag{11}$$

the charged particle can channel in a bent crystal. The minimum radius of curvature, $R_c = 1/\kappa_c$, at 7 TeV is 11.5 and 5.48 m for the (110) planes in Si and Ge, respectively. As κ_c is approached a rising fraction F, the so-called dechanneling fraction, is lost from the channeled states and is therefore unable to follow the curvature through the whole crystal.

4.2. Bending of Particle Beams

In consideration of the strong fields in a crystal it is understandable that a crystal has a superb bending power. One can calculate the equivalent magnetic field, $B = \kappa p/(Z_1 e)$, corresponding to the critical curvature κ_c as:

$$B_c[\mathrm{T}] = 1.5 \cdot 10^3 Z_2 \cdot n d_p \, [\text{Å}^{-2}]. \tag{12}$$

This critical field is $B_c \simeq 2500$ Tesla for a silicon crystal. Clearly, Equation (12) shows that a high-Z material is preferable for deflection.

4.3. Dechanneling

The length, L_D, over which a planar channeled beam of protons in a straight crystal has been reduced to the fraction 1/e of the initial intensity by transfer to non-channeled states by multiple scattering is given for $\gamma \gg 1$ by:

$$L_D = \frac{256}{9\pi^2} \frac{pv}{\ln(2\gamma mc^2/I_Z) - 1} \frac{a_s d_p}{Z_1 e^2}, \tag{13}$$

where I_Z is the ionisation potential. Equation (13) has been shown to be in good agreement with measured values of L_D at room temperature over a fairly wide range of energies. At 7 TeV, the values of L_D for Si and Ge are 2.9 m and 2.5 m which by far exceeds the dimensions of the crystals proposed for use. It appears from Equations (11) and (13) that heavy ions of the same momentum per charge pv/Z_2 to a first approximation (i.e. disregarding reactions that may probe the internal structure such as fragmentation) should behave like protons in bent crystals. Since heavy, fully stripped ions are composite particles of high charge a number of additional effects may appear, such as electromagnetic dissociation and/or nuclear interactions. In the restframe of the incident ion with the Lorentz factor $\gamma \simeq 160$ the extremely strong, crystal electric fields $\mathcal{E} \lesssim 10^{11}$ V/cm are boosted to very high values. It is thus not *a priori* excluded that electromagnetic dissociation for example through a giant dipole resonance is significant (Fusina and Kimball, 1987; Pivovarov et al., 1990). The fundamental frequency in the ion restframe for interaction with the lattice is $\omega_0 = 2\pi\gamma\beta c/d$ which is of the order 1 MeV for a characteristic lattice spacing $d \simeq 2$ Å.

4.4. Model for Deflection Efficiency

Since the straight crystal dechanneling favours small crystal lengths and the curvature favours long crystal lengths (for fixed angle), there is an optimum crystal length which depends on the angle and which is only weakly dependent on energy when the length is expressed in units of the dechanneling length. Given $\eta_F = F_D\kappa_c/\kappa \simeq 3$, where F_D is the dechanneling fraction, the approximate deflection efficiency is (Baurichter et al., 2000)

$$\varepsilon_{\text{appr.}} = \varepsilon_S \cdot e^{-L/L_D} \cdot \left(1 - \eta_F \frac{\theta}{(L/L_D)L_D\kappa_c}\left(1 + 2\frac{L}{L_D}\right)\right), \tag{14}$$

where

$$L_D\kappa_c = \frac{256}{9\pi} \frac{Z_2 N d_p^2 a_s}{\ln(2\gamma mc^2/I)} \tag{15}$$

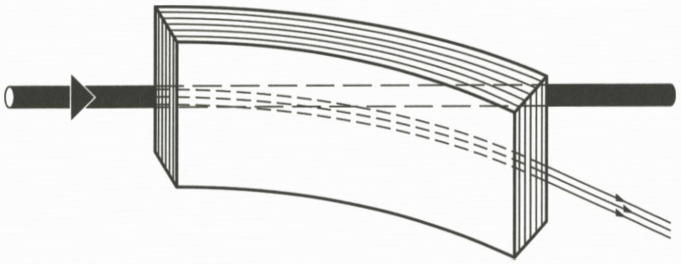

Figure 4. A schematical drawing of extraction of particles from the halo of a circulating beam by means of a bent crystal. From Møller (1995).

is only logarithmically dependent on energy and is 0.251 and 0.451 for Si and Ge along (110) at 7 TeV. Here L denotes the crystal length and the crystal is assumed to have a uniform curvature.

Equation (14) has a maximum at the optimum length

$$\frac{L}{L_{\mathrm{D}}} = -\frac{1+\sqrt{1-4\big(2-(L_{\mathrm{D}}\kappa_c/\eta_F\cdot\theta)\big)}}{2\big(2-(L_{\mathrm{D}}\kappa_c/\eta_F\cdot\theta)\big)} \tag{16}$$

with an efficiency value at this maximum of

$$\varepsilon_{\mathrm{max}}^{\mathrm{appr.}} \simeq \varepsilon_{\mathrm{S}}\left[\left(1-\sqrt{\frac{\eta_F\cdot\theta}{L_{\mathrm{D}}\kappa_c}}\right)^2 - 2\frac{\eta_F\cdot\theta}{L_{\mathrm{D}}\kappa_c}\left(1-\sqrt{\frac{\eta_F\cdot\theta}{L_{\mathrm{D}}\kappa_c}}\right)\right]. \tag{17}$$

As expected, heavy ions are deflected with equal efficiencies for the same momentum per charge – nuclear and electromagnetic interactions play a very minor role only (Uggerhøj et al., 2005a).

4.5. Extraction of Particles

Multi-pass extraction schemes yield extraction efficiencies that are higher than the single-pass extraction for beam divergencies larger than the planar critical angle. The reason is that particles that encounter the crystal and are not channeled will not necessarily be lost and may be extracted on a later turn in the machine. Furthermore, parameters of the accelerator lattice such as e.g. the betatron amplitude function that determines the beam size and divergence, become important for the extraction efficiency.

An actual implementation of a crystalline extraction device – in principle as shown in Figure 4 – at the coming LHC at CERN has recently been proposed

(Uggerhøj and Uggerhøj, 2005). This would enable a nearly continuous beam of 7 TeV protons extracted towards the LHC beam dump with an intensity of $\simeq 5{\cdot}10^8$ per second and a horizontal emittance as low as 20 μm·μrad.

4.6. Some Remaining Puzzles and Problems

The field of relativistic particle deflection in bent crystals is by now rather mature, with – in the opinion of the author – few big puzzles or questions left. For an application, though, the radiation sensitivity of the deflection process for heavy ions has never been investigated, while it is known that deterioration does not happen in high energy proton beams until a fluence of 10^{20}/cm^2. Most of the other aspects of the phenomenon are well described by the model calculations mentioned or by more elaborate simulations.

5. Radiative Energy Loss and Pair Production – Leptons and Photons

5.1. Interactions in Electromagnetic Fields

When passing matter, a photon can convert into an electron-positron pair in the electromagnetic field of a nucleus or a target electron. The presence of the external field is required to conserve energy and momentum in the creation process. Likewise, radiation emission can take place when a charged particle interacts with the external field.

By crossing symmetry pair production and radiation emission are two connected examples of the same physical process. One may for instance consider turning the Feynman diagram for bremsstrahlung a quarter of a turn to obtain the (simplified) diagram for pair production. Therefore the descriptions of the two processes are closely connected and e.g. their total cross sections differ only by a factor 7/9 due to different kinematic properties in the final state.

The radiation from relativistic particles is mainly propagating within a narrow cone of width $1/\gamma$ along the forward direction of the emitting particle. Based on the same mechanism, a pair created by a high energy photon is typically moving inside an angle $1/\gamma_p$ to the direction of the initial photon where γ_p is understood as $\hbar\omega/mc^2$. This typical value is of interest in connection with formation lengths to be discussed later.

In 1955, Dyson and Überall suggested the increase of bremsstrahlung emission for electrons penetrating e.g. a lead crystal close to a crystalline direction, compared to incidence along a random direction. This is in some sense a precursor to the strong field theory discussed below, since contrary to the following coherence theories, the enhancement along crystallographic directions was predicted to be

significantly larger than one. Shortly after their initial discovery, the theory of coherent bremsstrahlung and coherent pair production, was developed, see e.g. Palazzi (1968).

5.2. Strong Field Effects

At sufficiently high energies, however, a new phenomenon arises: strong field effects. The reason for this new behaviour at high energies can be seen as the possibility of achieving an enormously high field in the restframe of the emitting or produced particle. Emission and conversion probabilities can be calculated in this frame where the strong crystalline fields are Lorentz-boosted by γ and therefore become comparable to or even stronger than the critical field $\mathcal{E}_0 = m^2c^3/e\hbar = 1.32 \cdot 10^{16}$ V/cm. As Lindhard has phrased it: "[The electric forces on a channeled, relativistic electron in a single crystal has] an effect simulating that of an exceedingly large magnetic field of slowly varying magnitude" (Lindhard, 1991). Under small angles of incidence to a crystal, the strong electric fields of the nuclear constituents add coherently in the continuum approximation. Thus, a macroscopic, continuous field with a peak value of the order $\mathcal{E} \simeq 10^{11}$ V/cm is obtained. Therefore, in the restframe of an ultrarelativistic electron with a Lorentz factor of $\gamma \simeq 10^5$, the field encountered becomes comparable to the critical (or Schwinger-) field, $\mathcal{E}_0 = m^2c^3/e\hbar = 1.32 \cdot 10^{16}$ V/cm, corresponding to a magnetic field $B_0 = 4.41 \cdot 10^9$ T. The incident particle moves in these immensely strong fields over distances up to that of the crystal thickness, i.e. up to several mm. Since the quantity $\gamma\mathcal{E}/\mathcal{E}_0$ is a relativistic invariant, the behaviour of charged particles in strong fields as $\mathcal{E}_0$ can be investigated by use of ultrarelativistic electrons in strong crystalline fields. An introduction to these "strong field effects" can be found in Sørensen (1991) and Uggerhøj (2005).

5.3. Formation Lengths

As first discovered by Ter-Mikaelian, it takes relatively long time and therefore long distance for an energetic electron to create a photon. The interactions of the electron over this "formation zone" may affect the radiation spectrum destructively or constructively.

5.3.1. *Classical Formation Length*

One approach to derive the formation length, is to consider the photon "formed" by the time it takes for a photon to advance with respect to the electron by one

reduced wavelength, $\lambda/2\pi$ and by the corresponding distance of travel of the electron, l_f:

$$\frac{l_f}{v} = \left(l_f + \frac{\lambda}{2\pi}\right)\frac{1}{c}, \tag{18}$$

which for $v = \sqrt{(1 - 1/\gamma^2)}c \simeq c$ yields

$$l_f = \frac{2\gamma^2 c}{\omega}, \tag{19}$$

where v is the speed of the electron, c the speed of light and $\gamma = E/mc^2$ the Lorentz factor related to the energy of the electron, E, and its rest mass, m. Alternative methods – leading to the same result – can be found in Uggerhøj (2005).

5.3.2. *Quantum Formation Length*

In quantum theory, taking the recoil imposed on the electron by the emitted photon into account, the formation length can be calculated by use of the minimum longitudinal momentum transfer to the nucleus, $q_\parallel = p - p_f - \hbar\omega/c$. The photon propagates in a medium with velocity c/n_r and momentum $\hbar k_r = \hbar n_r k$ where $n_r = \sqrt{\varepsilon(\omega)} = \sqrt{1 - \omega_p^2/\omega^2}$ is the index of refraction, $\varepsilon(\omega)$ the dielectric function and $\omega_p = \sqrt{4\pi n Z e^2/m}$ the plasma frequency. By the uncertainty relation $l_f = \hbar/q_\parallel$ where p and p_f denote the momentum of the electron before and after the radiation event, respectively (Ter-Mikaelian, 1972) the formation length can be obtained.

The formation length under these conditions becomes:

$$l_f = \frac{2\gamma^2 c}{\omega^*} \quad \text{with} \quad \omega^* = \omega \cdot \frac{E}{E - \hbar\omega} \simeq \omega, \tag{20}$$

where $\hbar\omega$ is the energy of the photon.

5.4. Amorphous Targets

5.4.1. *The Bethe–Heitler Yields*

The cross section for radiation emission in an amorphous foil can be found from the Bethe–Heitler formula (Bethe and Heitler, 1934; Heitler, 1954) which is derived in perturbative QED and is approximately given by:

$$\frac{\mathrm{d}\sigma}{\mathrm{d}\hbar\omega} = \frac{16}{3} Z_2^2 \alpha r_e^2 \frac{1}{\hbar\omega}\left(1 - \frac{\hbar\omega}{E} + \frac{3}{4}\left(\frac{\hbar\omega}{E}\right)^2\right)\ln(183 Z_2^{-1/3}), \tag{21}$$

where $r_e = e^2/mc^2 = \alpha\lambda\!\!\!^{-} = \alpha^2 a_0$ is the classical electron radius, $\alpha = e^2/\hbar c$ the fine-structure constant, a_0 the Bohr radius and the logarithmic factor indicates complete screening, $\gamma \gg 1$. From this and the number density of atoms, n, the radiation length, X_0, can be found

$$\frac{1}{X_0} = N \int_0^E \frac{\hbar\omega}{E} \frac{\mathrm{d}\sigma}{\mathrm{d}\hbar\omega} \mathrm{d}\hbar\omega = 4Z_2^2 \alpha N r_e^2 \ln(183 Z_2^{-1/3}). \tag{22}$$

An incident particle statistically loses all but 1/e of its energy by emission of bremsstrahlung in passing a foil of thickness X_0. The radiation probability for emission with an energy between E and E_0 is found as

$$W = 1 - \exp(-\Delta t \cdot W_0) \tag{23}$$

with

$$W_0 = \int_{E_0}^E N \cdot \mathrm{d}\sigma \simeq \frac{4}{3}\frac{1}{X_0}\left(\ln\frac{E}{E_0} - \frac{5}{8}\right), \tag{24}$$

where Δt is the thickness of the foil where the radiation takes place and the approximation for W_0 is valid when the incident energy is much larger than the cut-off due to acceptance, $E \gg E_0$.

From W the probability of emitting two photons or more is calculated for $E \gg E_0$ according to a Poisson-distribution

$$f(N_\gamma) = \frac{p^{N_\gamma} e^{-p}}{N_\gamma!}, \tag{25}$$

where $p = \Delta t W_0(E, E_0)$ and N_γ is the number of photons.

In the above approach, the radiation produced by scattering off the target electrons has been neglected since this term is proportional to Z_2 and is small compared to Equation (21). A more accurate expression is thus obtained by replacing Z_2^2 by $Z_2(Z_2 + 1)$, in good agreement with data (Tsai, 1974).

For pair production, the Bethe–Heitler theory (Heitler, 1954) gives the number of pairs created per unit length, $N_p = N\sigma$, per relative energy of the electron/positron, $\xi_\pm = E_{e^\pm}/\hbar\omega$ as approximately:

$$\frac{\mathrm{d}N_p}{\mathrm{d}\xi_\pm} = \frac{16}{3} Z_2^2 \alpha r_e^2 N \left(\frac{3}{4} - \xi_\pm + \xi_\pm^2\right) \ln(183 Z_2^{-1/3}) \tag{26}$$

or by use of Equation (22) simply

$$\frac{\mathrm{d}N_p}{\mathrm{d}\xi_\pm} = \frac{1}{X_0}\left(\xi_+^2 + \xi_-^2 + \frac{2}{3}\xi_+\xi_-\right) \tag{27}$$

with the total yield

$$N_p = \int_0^1 \frac{\mathrm{d}N_p}{\mathrm{d}\xi_\pm}\,\mathrm{d}\xi_\pm = \frac{7}{9}\frac{1}{X_0}\,. \tag{28}$$

Note here the similarity between the cross sections for radiation emission and pair production, Equations (21) and (26), originating from the crossing symmetry of the processes.

The length over which a particle statistically scatters an RMS angle $1/\gamma$ in an amorphous material due to multiple Coulomb scattering is given approximately by

$$l_\gamma = \frac{\alpha}{2\pi} X_0, \tag{29}$$

where α is the fine-structure constant and X_0 the radiation length.

5.5. Radiation Emission and the LPM Effect in Amorphous Matter

The study of the Landau–Pomeranchuk–Migdal (LPM) effect was spurred by the finding of Ter-Mikaelian, that photon emission by an energetic electron and pair production by an energetic photon happen over a relatively large distance known as the formation length. The formation length extends over distances many orders of magnitude larger than interatomic spacings. The LPM effect is a suppression of the bremsstrahlung or pair production yield originating from multiple Coulomb scattering within the formation length (Migdal, 1956; Landau and Pomeranchuk, 1953b).

Several experiments have presented evidence for the LPM effect in amorphous targets (Hansen et al., 2004). Even at electron energies corresponding to $\gamma = 5 \cdot 10^4$ only a small fraction of photon energies are affected. Since the "threshold" below which the photon yield is suppressed increases approximately with the energy of the electron squared (see below), to get a substantial fraction of the full spectrum of photons affected by LPM suppression requires energies of 250 GeV ($\gamma = 5 \cdot 10^5$) and above (Hansen et al., 2003, 2004).

In crystals, the LPM effect was investigated experimentally in the late eighties (Bak et al., 1988) in the 10 GeV region and later for 150 GeV electrons (Baurichter et al., 1997).

The majority of radiation emission takes place within a cone of opening angle $1/\gamma$ to the direction of the electron. So destructive interference may result if the electron scatters outside this zone. Therefore, if the formation length exceeds the

length l_γ, the emission probability decreases or, put differently, the effective formation length shortens. Equation (20) combined with Equation (29) leads to the threshold of the LPM effect at energies:

$$\hbar\omega^{\mathrm{q}}_{\mathrm{LPM}} = \frac{E^2}{E + E_{\mathrm{LPM}}}\,; \quad \hbar\omega^{\mathrm{c}}_{\mathrm{LPM}} \simeq \frac{E^2}{E_{\mathrm{LPM}}}\,, \tag{30}$$

where

$$E_{\mathrm{LPM}} = \frac{mc^2 X_0}{4\pi a_0} = 7.684 \cdot X_0\ \mathrm{TeV/cm} \tag{31}$$

and a_0 is the Bohr radius. The value in parenthesis denotes the classical (recoilless) limit.

The LPM cross section for bremsstrahlung is given by Migdal as (Migdal, 1956; Landau and Pomeranchuk, 1953b; Klein, 1999):

$$\frac{\mathrm{d}\sigma_{\mathrm{LPM}}}{\mathrm{d}\hbar\omega} = \frac{4\alpha r_e^2 \xi(s)}{3\hbar\omega}\big(y^2 G(s) + 2[1 + (1-y)^2]\phi(s)\big) \times Z^2 \ln(184 Z^{-1/3}), \tag{32}$$

where $G(s)$, $\phi(s)$ and $\xi(s)$ are functions of $s = \sqrt{E_{\mathrm{LPM}}\hbar\omega/8E(E-\hbar\omega)\xi(s)}$, i.e. $\xi(s)$ is defined recursively, but can be well approximated, see e.g. Klein (1999). Here y denotes the fractional photon energy, $\hbar\omega/E$, Z the nuclear charge of the target and $r_e = \alpha^2 a_0$ the classical electron radius. In the limit $G(s) = \phi(s) = 1$ the Bethe–Heitler cross section is obtained. The Migdal expression, Equation (32), is relatively straightforward to implement in a Monte-Carlo simulation and compares well with experimental values.

Figure 5 shows an example of the measurements performed with 287 GeV electrons at CERN (Hansen et al., 2004). The aim of extending the accelerator based investigations by a factor 10 in energy compared to earlier experiments was twofold: To investigate a possible "compensation effect" proposed by Bell (1958) that would leave the effective radiation length unchanged (Hansen et al., 2003) and to explore the regime where the quantum recoil starts to become significant (Hansen et al., 2004). The experiment also provided a measurement of E_{LPM} for Cu, Ta and Ir by a comparison between data and simulated values where E_{LPM} was used as a free parameter. Subsequently, both Zakharov (2003) and Baier and Katkov (2004) calculated theoretical expectations which in both cases compared favourably to the experiment.

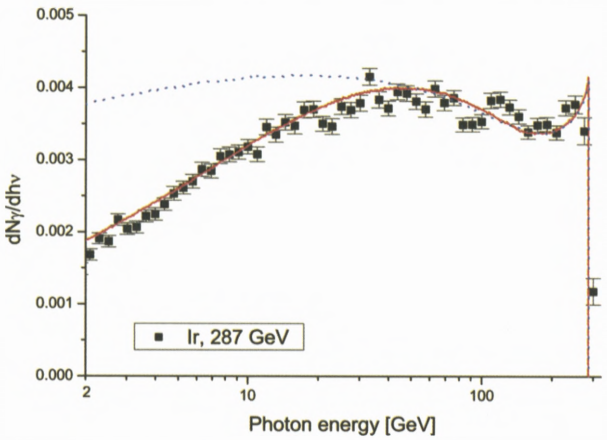

Figure 5. Photon energy spectra for 287 GeV e^- incident on a 4.4% X_0 Ir target. The filled squares with error bars are logarithmically binned measured values, the solid line is the simulated value including the LPM effect and the dotted line is the simulated value excluding the LPM effect, i.e. the Bethe–Heitler value. For details, see Hansen et al. (2003, 2004).

5.6. Pair Production and the LPM Effect in Amorphous Matter

Since pair-production can be considered the crossing-symmetry equivalent of photon emission, this process can be expected to be suppressed by the LPM mechanism as well. This has, however, not been verified experimentally.

For pair production, a classical version of the formation length is the length it takes to separate a created pair transversely by two Compton wavelengths, λ_c, when the pair is emitted with an opening angle $1/\gamma_p$:

$$l_{\mathrm{f}}^{\mathrm{pair}} = 2\gamma_p \lambda_c = \frac{2\gamma_p^2 c}{\omega}\,. \tag{33}$$

Therefore, the formation length increases with the energy of the pair (where $\gamma_p \equiv \hbar\omega/mc^2$).

When calculated properly by means of longitudinal momentum transfer, the formation length for pair production becomes:

$$l_{\mathrm{f}}^{rmpair} = \frac{2\gamma_p^2 c}{\omega^{\#}} \quad \text{with} \quad \omega^{\#} = \frac{\omega}{\eta_+ \eta_-}\,, \tag{34}$$

where $\eta_\pm$ is defined as $E_{\mathrm{e}^\pm}/\hbar\omega$ with $E_{\mathrm{e}^\pm}$ being the energy of the created electron or positron. It is an important distinction relevant to the Landau–Pomeranchuk–Migdal effect that l_{f} increases with increasing energy of the pair, whereas the

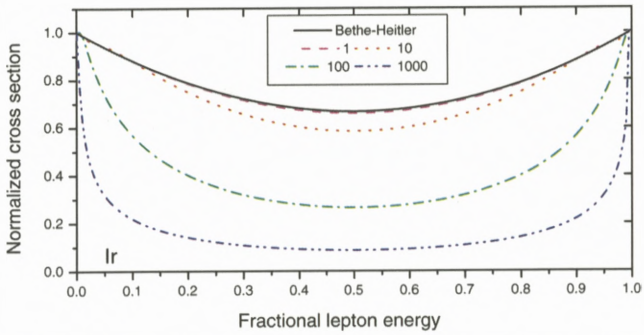

Figure 6. Calculated values for the normalized LPM pair production cross section $X_0 n\, \mathrm{d}\sigma/\mathrm{d}\eta$ where $\eta = E_{e^\pm}/\hbar\omega$ is the fractional energy of one lepton. The solid line is the Bethe–Heitler cross section, while (from the top) the dashed, dotted, dot-dashed and dot-dot-dashed correspond to photon energies $\hbar\omega$ =1, 10, 100 and 1000 TeV, respectively.

formation length for radiation emission decreases with increasing energy of the emitted photon for fixed energy of the radiating particle. On the other hand, the similarity between the two formation lengths when expressed as functions of γ, γ_p, ω^* and $\omega^\#$ reflect the crossing symmetry of the processes.

In the Migdal theory, the LPM cross section for pair production is given as (Migdal, 1956; Landau and Pomeranchuk, 1953b; Klein, 1999):

$$\frac{\mathrm{d}\sigma_{\mathrm{LPM}}}{\mathrm{d}\eta} = \frac{4\alpha r_e^2 \xi(\overline{s})}{3} \cdot \big(G(\overline{s}) + 2[\eta^2 + (1-\eta)^2]\phi(\overline{s})\big), \tag{35}$$

where $G(\overline{s})$, $\phi(\overline{s})$ and $\xi(\overline{s})$ are as given above, but functions of $\overline{s} = \sqrt{E_{\mathrm{LPM}}/8\eta\hbar\omega(1-\eta))\xi(\overline{s})}$. Again, in the limit $G(\overline{s}) = \phi(\overline{s}) = 1$ the Bethe–Heitler cross section is obtained.

As expected from Equation (34) symmetric pairs ($\eta_+ \simeq \eta_- \simeq 0.5$) are suppressed the most and to obtain a noticeable effect the photon energy must at least be of the order E_{LPM}.

From Figure 6 it is clear that even with a secondary beam of 4–5 TeV electrons derived from the 7 TeV proton beam of the LHC under construction at CERN, a measurement of the LPM effect in pair production is exceedingly demanding as the suppression amounts to a few percent only, even for symmetric pairs.

5.7. LPM Effects in Crystalline Matter

In the so-called continuum approximation (Lindhard, 1965), charged particles incident on a single crystal with small angles to crystallographic directions, experience the collective, screened nuclear fields as if smeared along the string or

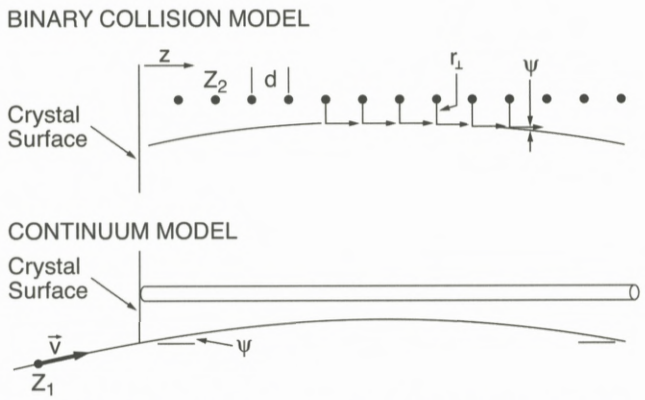

Figure 7. A schematical drawing of the discrete nature of the scattering centers in a crystal and the resulting continuum approximation.

plane, see Figure 7. For incidence with angles smaller than the so-called critical angle ψ_c, the particle has a low transverse momentum with respect to the axis or plane of the crystal. Thus it can be restricted to areas away from the nuclei (positively charged particles) or close to the nuclei (negatively charged particles). In this case the particle is channeled and is guided by the lattice such that a separation of the longitudinal and transverse motions is present. The result is a conserved "transverse energy" and therefore a transverse potential in which the particle moves. For an introduction to channeling at high energies, see e.g. Sørensen (1991) and Sørensen and Uggerhøj (1989).

The condition for the particle to be channeled is expressed by Lindhard's critical angle, ψ_c:

$$\frac{1}{2}pv\psi^2 \leq \frac{1}{2}pv\psi_c^2 = U_0 \;\Leftrightarrow\; \psi \leq \psi_c = \sqrt{\frac{2U_0}{pv}}\,, \tag{36}$$

where ψ is the angle to the crystallographic direction. Equation (36) states that the transverse energy must be smaller than the height of the transverse potential, U_0. The axial and planar critical angles are given by Lindhard as $\psi_1 = \sqrt{4Z_1Z_2e^2/pvd}$ and $\psi_p = \sqrt{4Z_1Z_2e^2Nd_pCa_s/pv}$ respectively, where Nd_p is the planar density of atoms, d the interaxial spacing, d_p the planar spacing, $C \simeq \sqrt{3}$ is Lindhard's constant and a_s is the (Thomas–Fermi) screening distance.

For incidence along an axial direction with somewhat larger angles $\psi_1 < \psi \lesssim 50\psi$, but still in the continuum approximation, the penetrating particle scatters off many strings of atoms, preserving the polar angle in each collision while changing the azimuthal angle in a stochastic fashion (Akhiezer et al., 1991).

The beam will reach an equilibrium state in azimuthal angles giving a uniform doughnut in angle space once the ensemble of particles has traversed a length given for $\psi \leq \psi_1$ by (Lindhard, 1965):

$$\lambda_{\perp}^{<} \simeq \frac{4\psi}{\pi^2 N \, \mathrm{d}a_s \psi_1^2} \tag{37}$$

and for $\psi \geq \psi_1$ roughly as (Bak et al., 1984; Andersen et al., 1980):

$$\lambda_{\perp}^{>} \approx 4\lambda_{\perp}^{<} \frac{\psi^2 u_1}{\psi_1^2 a_s}, \tag{38}$$

where u_1 is the one-dimensional thermal vibration amplitude of the lattice atoms. Doughnuts exist for angles much larger than ψ_1, implying that the continuum approximation is valid also for non-channeled, above-barrier particles. For a recent measurement of doughnuts, see Kirsebom et al. (2001b).

5.7.1. *Radiation Emission and the LPM Effect in Crystalline Matter*
The suppression due to doughnut scattering can be even more severe than due to multiple Coulomb scattering: If the particle is incident with a fixed angle ψ to the axis and deflects through an azimuthal angle ϕ, the change in angle becomes $\theta \simeq 2\psi \sin(\phi/2) \simeq \phi\psi$ and equating this with $2/\gamma$ an estimate for the length over which the particle scatters outside the radiation cone is obtained (Bak et al., 1988):

$$l_{\gamma\,\mathrm{d}} = \left(\frac{\phi}{2\pi}\right)^2 \lambda_{\perp} = \frac{\lambda_{\perp}}{\gamma^2 \psi^2 \pi^2}, \tag{39}$$

with $\lambda_{\perp}$ given by Equations (37) and (38) which denote the length required for the doughnut to develop fully. The length $l_{\gamma\,\mathrm{d}}$ can become smaller than l_{γ}, even along an axis where multiple Coulomb scattering is enhanced for negatively charged particles. Therefore suppression of radiation as well as for pair production can occur if the incident or produced particles doughnut scatter enough over one formation length to end outside the radiation cone.

The energy below which the radiation emission is suppressed by doughnut scattering can be estimated by use of Equations (20), (37), (38) and (39) as:

$$\hbar\omega \leq \hbar c \gamma^4 \pi^4 \psi_1^2 a_s \, \mathrm{d}N/2 \cdot \psi \tag{40}$$

for electrons inside the critical angle and:

$$\hbar\omega \leq \hbar c \gamma^4 \pi^4 \psi_1^4 a_s^2 \, \mathrm{d}N/8u_1 \cdot \psi^{-1} \tag{41}$$

outside the critical angle. Since $\psi_1^2 \propto 1/\gamma$ the doughnut scattering suppressions show a γ^3 and γ^2 dependence, respectively.

5.7.2. *Pair Production and the LPM Effect in Crystalline Matter*

The energy beyond which the pair production LPM suppression happens can be estimated by use of Equations (34), (37), (38) and (39) as:

$$\hbar\omega \geq \hbar\omega_{c\mathrm{d}}^{<} \simeq \frac{2mc^2}{\xi_+\xi_-\lambda_c\pi^4 N\,\mathrm{d}a_s\psi_1^2\gamma_p^2}\cdot\psi^{-1} \tag{42}$$

for pair production with the produced particles inside the critical angle and:

$$\hbar\omega \geq \hbar\omega_{c\mathrm{d}}^{>} \simeq \frac{8mc^2u_1}{\xi_+\xi_-\lambda_c\pi^4 N\,\mathrm{d}a_s^2\psi_1^4\gamma_p^2}\cdot\psi \tag{43}$$

for pair production with the produced particles outside the critical angle. Note that $\hbar\omega_{c\mathrm{d}}^{>}$ does not depend on γ_p since $\psi_1^2 \propto 1/\gamma$, but that $\psi_{\min} \simeq \psi_1$. As an example, consider the production of symmetric pairs along the $\langle 100\rangle$ axis in a diamond at room temperature – in this case $\hbar\omega_{c\mathrm{d}}^{>} \simeq \psi mc^2 \cdot 4 \cdot 10^9 \simeq 2$ GeV$\cdot\psi[\mu\mathrm{rad}]$ such that the effect should be observable down to ≈50 GeV. Likewise, for Ge $\langle 110\rangle$ the effect should extend down to ≈180 GeV for incidence outside ψ_1 and down to ≈80 GeV for incidence of a 150 GeV photon inside ψ_1 where the critical angle is calculated for a positron of the same energy. The effect of the reduced formation length in a strong field has not been taken into account, i.e. the formulas have been found for $\chi \leq 1$. More details can be found in Uggerhøj (2004).

Another effect of the LPM type is the reduction of the incoherent contribution due to coherent effects (Kononets, 1999; Tikhomirov, 1987a; Baier and Katkov, 2006). It is analogous to the self-suppression effect as a result of the diminishing formation length in a strong crystalline field, only in this case the suppression is of the incoherent contribution.

It is clear from Figure 6 that the LPM suppression in pair production for presently available accelerator energies is negligible. Even for a near future few-TeV electron beam generating bremsstrahlung photons, an experimental assessment would be extremely demanding. However, crystals may in fact present a possibility for measuring LPM suppression in pair production with beams in the few-hundred GeV region available today. The main reason is that the photon conversion into pairs in an aligned crystal predominantly takes place where the field is strongest, i.e. at small transverse distances from the string of nuclei, $r_\perp \simeq u_1$. At this transverse location, also the multiple Coulomb scattering is drastically increased - by up to three orders of magnitude! For this reason, one may expect the threshold for LPM suppression to decrease by approximately the same three orders of magnitude corresponding to a replacement of TeV by GeV. However, it is only the incoherent contribution that becomes suppressed and since the coherent contribution quickly dominates the pair production cross section, the

strong incoherent suppression becomes a small correction to the total yield *except* near the threshold for strong field effects where the incoherent contribution plays a significant role (Baier and Katkov, 2005).

5.8. Thin Targets – Ternovskii–Shul'ga–Fomin Effect

The formation length for radiation emission increases as shown with decreasing photon frequency. Thus, at a certain point the formation zone extends beyond the thickness of the foil. In this case, the radiation yield also becomes suppressed. Studies of this effect were first performed by Ternovskii and later extended by Shul'ga and Fomin and others. The first confirmation was obtained in experiments performed at SLAC (for references, see Uggerhøj et al., 2005c).

As to the extent of the effect, the analysis is applicable for target thicknesses $l_\gamma < \Delta x < l_\mathrm{f}$, see e.g. Shul'ga and Fomin (1998). Therefore, by use of Equation (20) and setting $\Delta x = l_\mathrm{f}/k_\mathrm{f}$ the effect appears for photon energies

$$\hbar\omega_\mathrm{TSF} = \frac{E}{1 + k_\mathrm{f}\Delta x/2\gamma\lambda_c}, \tag{44}$$

where $k_\mathrm{f} > 1$. The threshold of the effect is located at $k_\mathrm{f} = 1$, i.e. for $E/(1 + \Delta x/2\gamma\lambda_c)$.

The magnitude of the effect is evaluated from the averaged radiation spectrum (Shul'ga and Fomin, 1998)

$$\left\langle \frac{\mathrm{d}E}{\mathrm{d}\hbar\omega} \right\rangle \simeq \frac{2\alpha}{\pi}\left(\ln\frac{\Delta x}{l_\gamma} - 1\right) \tag{45}$$

and since for the Bethe–Heitler case

$$\left\langle \frac{\mathrm{d}E}{\mathrm{d}\hbar\omega} \right\rangle = \frac{4\Delta x}{3X_0},$$

the suppression factor, κ, can conveniently be expressed as

$$\kappa \simeq \frac{k_\gamma}{6(\ln k_\gamma - 1)}, \tag{46}$$

where $\Delta x = k_\gamma l_\gamma$ and $k_\gamma > 1$. As an example, for $\Delta x = 4.4\% X_0$ and $E = 287$ GeV, $k_\gamma = 0.044 \cdot 4\pi/\alpha \simeq 76$ yielding a suppression $\kappa = 3.8$, but for photon energies lower than $\hbar\omega_\mathrm{TSF} = 0.9$ GeV in Ir and 0.2 GeV in Cu.

5.9. Dielectric Suppression – Ter-Mikaelian Effect

In a medium with index of refraction, n, the velocity c/n replaces the photon velocity c. By use of this replacement in Equation (18) and the index of refraction expressed as $n = 1 - \omega_p^2/2\omega^2$, a modified formation length is obtained

$$\frac{1}{l_{\mathrm{f}\varepsilon}} \simeq \frac{\omega}{2\gamma^2 c} + \frac{\omega_p^2}{2\omega c} = \frac{1}{l_{\mathrm{f}}} + \frac{1}{l_{\mathrm{df}}}, \tag{47}$$

where $\omega_p = \sqrt{4\pi N Z e^2/m}$ is the plasma frequency, NZ being the electron density. The inverse of the dielectric formation length, $l_{\mathrm{df}} = 2\omega c/\omega_p^2$, becomes dominating in Equation (47) for photon energies below the value

$$\hbar\omega_{\mathrm{d}} = \gamma\hbar\omega_p. \tag{48}$$

Therefore – in close analogy with the density effect in ionization energy loss – formation lengths beyond l_{df} are effectively cut off. Thus, for photon energies in the regime below $\hbar\omega_{\mathrm{d}}$ the photon yield is suppressed by the Ter-Mikaelian effect, also known as dielectric suppression or the longitudinal density effect, see e.g. Ter-Mikaelian (1972). However, as plasma frequencies are of the order 50 eV/$\hbar$, even electron energies as high as 287 GeV in iridium leads to a suppression only below $\hbar\omega_{\mathrm{d}} = 86$ MeV.

5.10. Some Remaining Puzzles and Problems

For the subject of radiative energy loss and pair production, the inhibiting effects have almost all been studied experimentally for the radiation emission case only. For the LPM suppression, as mentioned, an experimental test in amorphous materials for pair production would require extreme attention to detail, even for a 1 TeV photon beam. However, use of the fact that multiple scattering is strongly increased in crystals may be utilized to reduce this energy scale by about three orders of magnitude.

New initiatives include the investigations of structured or sandwich-targets, where many thin foils are spaced small distances – corresponding to the formation length for a particular photon energy – apart. The spacers are typically chosen with as long a radiation length as possible, e.g. low density polyethylene. From such arrangements of targets, resonances should appear as predicted by theory (Blankenbecler, 1997a, 1997b; Baier and Katkov, 1999).

Contemporary research in the field of relativistic beams in crystals, is pursuing the first detection of so-called crystalline undulator radiation. This type of radiation is achieved by passing positrons of e.g. 10 GeV through a crystal

that has been manipulated to a sinusoidal shape in the direction transverse to the beam propagation, see e.g. Mikkelsen and Uggerhøj (2000). It is hoped that even self-amplified stimulated emission may someday be a possibility, leading to MeV photon beams of unprecedented brillance (Korol et al., 2004).

6. Conclusion

As shown in this review, there are still many intriguing questions and puzzles to be pursued within the subject of penetration phenomena for relativistic beams. Although at first sight many of the mentioned effects may seem of secondary importance, some of them are actually necessary ingredients to understand e.g. the efficiency of calorimeters at the next generation of particle physics experiments or the behaviour connected with detection of giant air showers as e.g. in the Pierre Auger Observatory, presently under commissioning in Argentina.

Acknowledgement

It is a pleasure to thank P. Sigmund for the invitation to Ion06, held in an extraordinarily beautiful setting, as well as for his kind encouragement to write this review.

References

Akhiezer A.I. and Shul'ga N.F. (1996): High Energy Electrodynamics in Matter, Gordon and Breach

Akhiezer A.I., Truten V.I. and Shul'ga N.F. (1991): Dynamic chaos in the motion of charged particles through a crystal. Phys Rep **203**, 289–343

Andersen S.K. et al. (1980): Influence of channeling on scattering of 2–15 GeV/c protons, π^+, and π^- incident on Si and Ge crystals. Nucl Phys B **167**, 1–40

Baier V.N. and Katkov V.M. (1999): Landau–Pomeranchuk–Migdal effect and transition radiation in structured targets. Phys Rev D **60**, 076001

Baier V.N. and Katkov V.M. (2004): Variation of radiation length due to LPM effect. Phys Lett A **327**, 202–209

Baier V.N. and Katkov V.M. (2005): Coherent and incoherent pair creation by a photon in oriented single crystal. Phys Lett A **346**, 359–366

Baier V.N. and Katkov V.M. (2006): Coherent and incoherent radiation from high-energy electron and the LPM effect in oriented single crystal. Phys Lett A **353**, 91–97

Bak J.F. et al. (1984): Detailed investigation of the channeling phenomena involved in bending of high-energy beams by means of crystals. Nucl Phys B **242**, 1–30

Bak J.F. et al. (1988): Channeling radiation from 2 to 20 GeV/c electrons and positrons, (II) axial case. Nucl Phys B **302**, 525–558

Baurichter A. et al. (1997): Radiation emission and its influence on the motion of multi-GeV electrons and positrons in strong crystalline fields. Phys Rev Lett **79**, 3415–3418

Baurichter A. et al. (2000): Channeling of high-energy particles in bent crystals – Experiments at the CERN SPS. Nucl Instr Meth B **164–165**, 27–43

Bell J.S. (1958): Bremsstrahlung from multiple scattering. Nucl Phys **8**, 613–620

Berestetskii V.B. and Geshkenbain B.V. (1957): Ionizational slowing down of high-energy electron positron pairs. Sov Phys JETP **4**, 609–610

Bethe H. and Heitler W. (1934): On the stopping of fast particles and on the creation of positive electrons. Proc Roy Soc A **146**, 83–112

Blankenbecler R. (1997a): Structured targets and the Landau–Pomeranchuk–Migdal effect. Phys Rev D **55**, 190–195

Blankenbecler R. (1997b): Multiple scattering and functional integrals. Phys Rev D **55**, 2441–2448

Datz S. et al. (1996): Effect of nuclear size on the stopping power of ultrarelativistic heavy ions. Phys Rev Lett **77**, 2925–2928

Dyson F.J. and Überall H. (1955): Anisotropy of bremsstrahlung and pair production in single crystals. Phys Rev **99**, 604–605

Esbensen H. and Golovchenko J.A. (1978): Energy loss of fast channeled particles. Nucl Phys A **298**, 382–396

Esbensen H. et al. (1978): Random and channeled energy loss in thin germanium and silicon crystals for positive and negative 2 – 15-GeV/*c* pions, kaons, and protons. Phys Rev B **18**, 1039–1054

Fusina R. and Kimball J.C. (1987): Resonant excitation of fast nuclei in crystals. Nucl Instr Meth B **27**, 368–373

Hansen H.D., et al. (2003): Is the electron radiation length constant at high energies? Phys Rev Lett **91**, 014801

Hansen H.D., et al. (2004): The LPM effect for multi-hundred GeV electrons. Phys Rev D **69**, 032001

Heitler, W. (1954): The Quantum Theory of Radiation. Dover, New York

Jackson J.D. (1975): Classical Electrodynamics. John Wiley, New York

Jain P.L. (1962): Nucleon-nucleon interactions at energies greater than 10^{12} eV. Phys Rev **125**, 679–687

Jeanneret J.B. (1998): Optics of a two-stage collimation system. Phys Rev ST Accel Beams **1**, 081001

Jowett J.M., Jeanneret J.-B. and Schindl K. (2003): Heavy ion beams in the LHC. In: Proceedings Particle Accelerator Conference, Vol. 3, pp 1682–1684

Klein S. (1999): Suppression of bremsstrahlung and pair production due to environmental factors. Rev Mod Phys **71**, 1501–1538

Kirsebom K., et al. (2001b): Radiation emission and its influence on the motion of multi-GeV electrons and positrons incident on a single diamond crystal. Nucl Instr Meth B **174**, 274–296

Kononets Yu.V. (1999): The basic QED processes in strong crystalline fields – Selected topics of recent developments. In: Pisin Chen (Ed.), Quantum Aspects of Beam Physics, Monterey 1998. World Scientific

Korol A.V., Solov'yov A.V. and Greiner W. (2004): Channeling of positrons through periodically bent crystals: On the feasibility of crystalline undulator and gamma-laser. Int J Mod Phys E **13**, 867–916

Krause H. et al. (2001): Electron capture and ionization of 33-TeV Pb ions in gas targets. Phys Rev A **63**, 032711

Landau L.D. and Pomeranchuk I.J. (1953b): Electron-cascade processes at ultra-high energies. Dokl Akad Nauk SSSR **92**, 735 [English translation available in Landau, L.D. (1965): The Collected Papers of L.D. Landau. Pergamon, New York, pp 589–593]

Lindhard J. (1965): Influence of crystal lattice on motion of energetic charged particles. K Dan Vidensk Selsk Mat Fys Medd **34, no. 14**, 1–64

Lindhard J. (1991): Quantum-radiation spectra of relativistic particles derived by the correspondence principle. Phys Rev A **43**, 6032–6037

Lindhard J. and Sørensen A.H. (1996): Relativistic theory of stopping for heavy ions. Phys Rev A **53**, 2443–2456

Mandal S.K., Klein S.R. and Jackson J.D. (2005): Cherenkov radiation from e^+e^- pairs and its effect on ν_e induced showers. Phys Rev D **72**, 093003

Migdal A.B. (1956): Bremsstrahlung and pair production in condensed media at high energies. Phys Rev **103**, 1811–1820

Mikkelsen U. and Uggerhøj E. (2000): A crystalline undulator based on graded composition strained layers in a superlattice. Nucl Instr Meth B **160**, 435–439

Møller S.P. (1995): High-energy channeling – Applications in beam bending and extraction. Nucl Instr Meth A **361**, 403–420

Møller S.P. et al. (2001): Random and channeled energy loss of 33.2 TeV Pb nuclei in silicon single crystals. Phys Rev A **64**, 032902

Palazzi G.D. (1968): High-energy bremsstrahlung and electron pair production in thin crystals. Rev Mod Phys **40**, 611

Perkins D.H. (1955): Ionization at the origin of electron pairs, and the lifetime of the neutral pion. Phil Mag **46**, 1146–1148

Pivovarov Yu.L., Shirokov A.A. and Vorobiev S.A. (1990): Coherent electromagnetic excitation and disintegration of relativistic nuclei passing through crystals. Nucl Phys A **509**, 800–822

Scheidenberger C. et al. (2002): Electromagnetically induced nuclear-charge pickup observed in ultrarelativistic Pb collisions. Phys Rev Lett **88**, 042301

Scheidenberger C. et al. (2004): Charge-changing interactions of ultrarelativistic nuclei. Phys Rev C **70**, 014902

Shul'ga N.F. and Fomin S.P. (1998): Effect of multiple scattering on the emission of ultrarelativistic electrons in a thin layer of matter. Sov Phys JETP **86**, 32–38

Sigmund P. (2006): Particle Penetration and Radiation Effects. Springer

Sørensen A.H. (1991): Channeling, bremsstrahlung and pair creation in single crystals. In: Fried H.M. and Müller B. (Eds), Vacuum Structure in Intense Fields, NATO ASI, Vol. 255, Plenum Press, New York, pp 91–118 [Reprinted in: Channeling, bremsstrahlung and pair creation in single crystals. Nucl Instrum Meth B **119**, 2–29 (1996)]

Sørensen A.H. (2003): Stopping of relativistic heavy ions; the pair production and bremsstrahlung channels. AIP Conf Proc **680**, 102–105

Sørensen, A.H. (2005): Pair production and bremsstrahlung contributions to the stopping of relativistic heavy ions. Nucl Instr Meth B **230**, 12–16

Sørensen A.H. and Uggerhøj E. (1989): Channeling, radiation and applications. Nucl Sci Appl **3**, 147

Ter-Mikaelian M.L. (1972): High-Energy Electromagnetic Processes in Condensed Media. Wiley Interscience, New York

Ter-Mikaelian M.L. (2001): Electromagnetic radiative processes in periodic media at high energies. Map Fiz Nauk **171**, 597–624 [Sov Phys Usp **44**, 571–596 (2001)]

Tikhomirov V.V. (1987a): The position of the peak in the spectrum of 150 GeV electron energy losses in a thin germanium crystal is proposed to be determined by radiation cooling. Phys Lett A **125**, 411–415

Tsai Y. (1974): Pair production and bremsstrahlung of charged leptons. Rev Mod Phys **46**, 815–851; Erratum (1977): Rev Mod Phys **49**, 421–423

Uggerhøj U.I. (2004): The Landau–Pomeranchuk–Migdal effect for amorphous and crystalline matter. Mod Phys Lett B **18**, 309–325

Uggerhøj U.I. (2005): The interaction of relativistic particles with strong crystalline fields. Rev Mod Phys **77**, 1131–1171

Uggerhøj U.I. and Uggerhøj, E. (2005): Strong crystalline fields – A possibility for extraction from the LHC. Nucl Instr Meth B **234**, 31–39

Uggerhøj U.I. et al. (2005a): Strong suppression of nuclear-charge changing interactions for 18 TeV/c In ions channeled in a bent Si crystal. Phys Lett B **619**, 240–246

Uggerhøj U.I. et al. (2005b): Charge-changing interactions of ultrarelativistic in nuclei. Phys Rev C **72**, 057901

Uggerhøj U.I. et al. (2005c): Formation length effects in very thin targets. Phys Rev D **72**, 112001

Yao W.-M. et al. (2006): Review of particle physics. J Phys G **33**, 1+

Zakharov B.G. (2003): Description of the CERN SPS data on the Landau–Pomeranchuk–Migdal effect for photon bremsstrahlung in the quantum regime. Sov Phys JETP Lett **78**, 759–762

Zielinski I.P. (1985): On the possibility of the electronic measurement of the King–Perkins–Chudakov effect for electron pairs using a multilayer silicon detector. Nucl Instr Meth A **238**, 562–563